

Jarosław SEP*, Leszek TOMCZEWSKI*, Lidia GAŁDA*

THE EFFECT OF HELICAL GROOVE PRESENCE ON THE TRIBOLOGICAL PERFORMANCE OF JOURNAL BEARINGS

WPLYW SPIRALNEGO ROWKA NA CHARAKTERYSTYKI STATYCZNE ŁOŻYSK ŚLIZGOWYCH

Key words:

groove geometry, grooved journal bearings, steady-state.

Abstract

The hydrodynamic bearings could suffer critical damages operating in contaminated environments that cause machine breakdown. In such hard operating conditions, hydrodynamic bearings with grooved journals are less sensitive to damage compared to plain bearings. The wear resistance of the grooved journal bearings is several times greater than that of smooth journal bearings. Contaminants existing in the oil film are moved out from the bearing clearance by the groove created on the journal surface.

The presence, shape, and geometry of the groove strongly influence the bearings performance. The aim of this article is to study the selected static characteristics of bearings consisting of a journal with the helical groove on its surface. The static characteristics were determined based on the flow simulation in the oil clearance. A three-dimensional, adiabatic model of the oil flow was assumed. The oil flow was described with the Navier-Stokes continuity and energy equations. The equation system was solved by the finite volume method. The numerical model of the flow was verified experimentally on a test stand. It has been established that the grooved journal application leads to a decrease of load capacity in whole range of eccentricity and for all examined clearances. The oil flow rate increase was mainly observed due to spiral groove presence on the shaft.

Słowa kluczowe:

kształt rowka, łożysko ślizgowe z rowkiem, stan ustalony.

Streszczenie

Hydrodynamiczne łożyska ślizgowe pracujące w zanieczyszczonym środowisku narażone są na poważne uszkodzenia powodujące awarie maszyn. W trudnych warunkach pracy można zastosować łożyska ślizgowe ze spiralnym rowkiem na powierzchni czopa, zmniejszając ich wrażliwość na uszkodzenia przez cząstki ściernie. Odporność na zużycie łożysk ze spiralnym rowkiem jest kilka razy większa w porównaniu ze zużyciem gładkich łożysk ślizgowych. Zanieczyszczenia w filmie olejowym są odprowadzane ze strefy tarcia na zewnątrz łożyska poprzez rowek.

Obecność, kształt i wymiary rowka wpływają znacząco na charakterystyki łożyska. Celem artykułu jest przedstawienie charakterystyk statycznych łożysk ślizgowych z ukształtowanym rowkiem na powierzchni czopa. Badania symulacyjne zrealizowano w oparciu o adiabatyczny, przestrzenny model przepływu oleju w szczelinie smarowej. Przepływ oleju został opisany równaniami Naviera-Stokesa, ciągłości i energii. Do obliczeń zastosowano metodę objętości skończonych w programie ANSYS Fluent. Model numeryczny został zweryfikowany eksperymentalnie. W wyniku przeprowadzonych badań stwierdzono, że zastosowanie spiralnego rowka powoduje zmniejszenie nośności łożyska i wartości maksymalnej temperatury oleju. Łożyska z rowkiem charakteryzowały się większym wydatkiem oleju w porównaniu z łożyskami gładkimi.

INTRODUCTION

Due to the cavitation effect, the spiral or herringbone grooved journal bearings obtained better performance in comparison to smooth bearings [L. 1–3]. Such grooved

journal bearings were applied in high-speed and low-loaded devices because of their great reliability, stable, and also leakage-free operation [L. 4, 5]. Over a two-fold decrease in the journal wear in comparison to that of plain journal was due to the presence of a helical groove

* Faculty of Mechanical Engineering and Aeronautics, Rzeszów University of Technology, Powstańców Warszawy 12, 35-959 Rzeszów, Poland.

on the journal's surface [L. 6]. The surface topography analysis showed that contaminants were removed from the bearing clearance and very small concentrations of contaminants were found after abrasive wear tests [L. 7].

In literature, there are numerous numerical investigations on the effect of groove or texture in different shapes and configurations on bearing performance. Tala and Fillon [L. 8] found that fully texturing the bearing surface improved the hydrodynamic characteristics only at very low journal rotational speeds while partially texturing at the outlet of the active pressure zone resulted in higher improvement of the bearing. Deep theoretical examinations of full and partial surface texturing in journal bearings were done by Brizmer and Kligerman. The beneficial effect of partial texturing in the load capacity increase was obtained when the eccentricity ratio was in the range of 0.1 to 0.3 [L. 9]. Tonder also theoretically examined the dynamic characteristics of tribodevices taking into account the inlet roughness for longitudinal and transverse grooves. For devices where thin film is expected, the grooves may increase stiffness and damping and decrease the leakage [L. 10]. Fundamental analyses of surfaces texturing applying in different mechanical components were conducted by Etsion [L. 11–13]. In most of the investigations, the Reynolds equations were solved, because they have shown good agreement with experimental results. However, in several cases, when the texture was characterized by a large aspect ratio (depth over diameter or width), the full Navier-Stokes equations should be employed [L. 12].

The main goal of this study was to find the static characteristics for grooved journal bearings that were more resistive to abrasive wear in comparison to conventional journal bearing wear [L. 6, 14]. The investigations were concentrated on the effect of the eccentricity and clearance of grooved and plain bearings on the load carrying capacity, oil flow rate, maximum pressure, and maximum oil temperature.

EXPERIMENTAL AND NUMERICAL PROCEDURE

Numerical model

The computer simulations were realized for the bearing clearance filled with the clean oil without any contaminants, because a high concentration of contaminants in the lubricated substance is only considered as the emergency situations or in specific applications. As a standard, the bearings and their lubrication systems are designed for operation in the oil without any distinct particles. The computer investigations presented in this paper consider the operating conditions without any presence of contaminants in the bearing clearance.

Based on the previous investigations [L. 15, 16] and due to the high aspect ratio of the groove dimensions, the Navier-Stokes equations were applied to describe the oil film behaviour in the journal bearings. In the previous investigation [L. 15, 16], the differences between modelled and experimental pressure values were up to 12% in the case of smooth journals and 14% for spiral grooved journals. In this study, the numerical investigations of the load bearing capacity were also done for the clean oil film in slide bearings with the spiral groove on its surface and with a plain surface. Computer calculations were based on the finite volume method. In the physical model of the journal bearing clearance, it was assumed that shaft and bearing were without any deformations. Shaft and bearing surfaces were ideally smooth besides shafts zones that contain spiral grooves with a specified geometry. The axis of the shaft and bearing were parallel. The mating of the shaft and bearing was separated by oil in which viscosity and density depended on temperature (Newtonian oil). The oil flow in the bearing clearance was laminar and heat was distributed by the oil (adiabatic model). Reynolds boundary conditions on pressure were assumed (pressure is greater or equal to zero). Feeding and pressure were constant.

To solve the problem and taking into account the assumptions listed above, the Navier-Stokes equations (1) describing the flow, the mass continuity (2), energy (3), and function of energy dissipation (4) equations were applied:

$$\begin{aligned} \rho \left(u_r \frac{\partial u_r}{\partial r} + \frac{u_\theta}{r} \frac{\partial u_r}{\partial \theta} - \frac{u_\theta^2}{r} + u_z \frac{\partial u_r}{\partial z} \right) \\ = - \frac{\partial p}{\partial r} + \eta \left(\frac{1}{r} \frac{\partial}{\partial r} \left(r \frac{\partial u_r}{\partial r} \right) - \frac{u_r}{r^2} + \frac{1}{r^2} \frac{\partial^2 u_r}{\partial \theta^2} - \frac{2}{r^2} \frac{\partial u_\theta}{\partial \theta} + \frac{\partial^2 u_r}{\partial z^2} \right) \\ \rho \left(u_r \frac{\partial u_\theta}{\partial r} + \frac{u_\theta}{r} \frac{\partial u_\theta}{\partial \theta} + \frac{u_r u_\theta}{r} + u_z \frac{\partial u_\theta}{\partial z} \right) \\ = - \frac{1}{r} \frac{\partial p}{\partial \theta} + \eta \left(\frac{1}{r} \frac{\partial}{\partial r} \left(r \frac{\partial u_\theta}{\partial r} \right) - \frac{u_\theta}{r^2} + \frac{1}{r^2} \frac{\partial^2 u_\theta}{\partial \theta^2} + \frac{2}{r^2} \frac{\partial u_r}{\partial \theta} + \frac{\partial^2 u_\theta}{\partial z^2} \right) \end{aligned} \quad (1)$$

$$\rho \left(u_r \frac{\partial u_z}{\partial r} + \frac{u_\theta}{r} \frac{\partial u_z}{\partial \theta} + u_z \frac{\partial u_z}{\partial z} \right) = - \frac{\partial p}{\partial z} + \eta \left(\frac{1}{r} \frac{\partial}{\partial r} \left(r \frac{\partial u_z}{\partial r} \right) + \frac{1}{r^2} \frac{\partial^2 u_z}{\partial \theta^2} + \frac{\partial^2 u_z}{\partial z^2} \right)$$

$$\frac{1}{r} \frac{\partial (r u_r)}{\partial r} + \frac{1}{r} \frac{\partial (u_\theta)}{\partial \theta} + \frac{\partial u_z}{\partial z} = 0 \quad (2)$$

$$\rho c \left(u_r \frac{\partial T}{\partial r} + \frac{u_\theta}{r} \frac{\partial T}{\partial \theta} + u_z \frac{\partial T}{\partial z} \right) = k \left(\frac{1}{r} \frac{\partial}{\partial r} \left(r \frac{\partial T}{\partial r} \right) + \frac{1}{r^2} \frac{\partial}{\partial \theta} \left(\frac{\partial T}{\partial \theta} \right) + \frac{\partial}{\partial z} \left(\frac{\partial T}{\partial z} \right) \right) + \eta \Phi \quad (3)$$

$$\Phi = \left\{ 2 \left[\left(\frac{\partial u_r}{\partial r} \right)^2 + \left(\frac{\partial u_\theta}{\partial r} \right)^2 + \left(\frac{\partial u_z}{\partial r} \right)^2 \right] + \left(\frac{1}{r} \frac{\partial u_r}{\partial \theta} + \frac{\partial u_\theta}{\partial r} \right)^2 + \left(\frac{\partial u_\theta}{\partial z} + \frac{1}{r} \frac{\partial u_z}{\partial \theta} \right)^2 + \left(\frac{\partial u_z}{\partial r} + \frac{\partial u_r}{\partial z} \right)^2 \right\} \quad (4)$$

The model of bearing clearance was built with the standard code of ANSYS Fluent program application. As a model, the Pressure-Velocity Coupling was chosen to derive the additional condition for pressure by reformatting the continuity equation. To enforce a mass conservation and to obtain a pressure field, the SIMPLE algorithm was applied. This Solution Method uses a relationship between velocity and pressure corrections [L. 17]. Regression functions describing dependencies of an oil viscosity and a density from a temperature were obtained experimentally, and the functions of temperature are presented in Formulas (5) and (6). The values of viscosity and density measured at selected temperatures were introduced into ANSYS software as user defined functions.

$$\eta = 4 \cdot 10^{28} \cdot T^{-12.02} \quad [\text{Pa} \cdot \text{s}] \quad (5)$$

$$\rho = -0.0071 \cdot T^2 + 3.9143 \cdot T + 341.07 \quad [\text{kg/m}^3] \quad (6)$$

The pressure at the oil inlet and on both sides of the bearing were set to ambient temperature at the oil inlet which was 293 K. The shaft was rotating at specific speed $n = 600$ rpm and the bearing was stationary $u = v = w = 0$. The eccentricity index ε was considered in the range of 0.1 – 0.8.

Two geometrical series were modelled and compared: the first was the journal bearing with smooth shaft, and the second was the one with groove on journal surface. The groove was created in spiral mode with the lead equal to 16 mm. The groove depth was 0.079 mm and its width was 0.5 mm.

EXPERIMENTAL DETAILS

In order to verify the simulation results, some experiments were conducted with the special stand application. The scheme and photo of the stand for journal bearing tests are presented in Fig. 1.

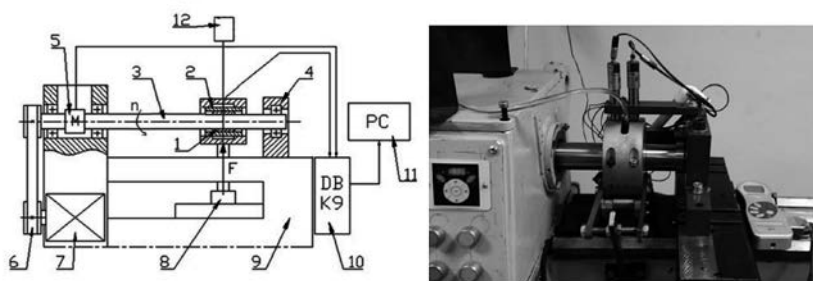


Fig. 1. Scheme of the stand (a) and photo of testing head (b) for journal bearing tests: 1 – bearing, 2 – bearing bush, 3 – shaft, 4 – support, 5 – torque gauge, 6 – belt gear, 7 – electric engine, 8 – hydraulic lift, 9 – housing, 10 – transducer, 11 – computer, 12 – oil reservoir

Rys. 1. Schemat stanowiska (a) i zdjęcie głowicy (b) do badań łożysk ślizgowych: 1 – panew, 2 – czop, 3 – wał, 4 – podpora, 5 – momentomierz, 6 – pas, 7 – silnik, 8 – siłownik, 9 – korpus, 10 – przetwornik sygnałów, 11 – komputer, 12 – zbiornik oleju

The experimental verification of simulation results were carried out for the smooth journal bearing at specific speed of 600 rpm and loads in the range of 500 – 2400 N (specific load 0,32 – 1,52 MPa). The examined journal was made from 42CrMo4 steel of 52 HRC hardness after heat treatment. The bearing was made of CuSn10P alloy.

The geometrical and operating conditions of the examined journal bearings were as follows:

- Journal diameter: $d = 52.7$ mm,
- Bearing length: $L = 30$ mm,
- Bearing length to diameter ratio: $L/D = 0.56$,
- Radial clearance ratio: $\psi = 0.002$,
- The rotational speed of journal: $n = 600$ rpm ($v = 1.65$ m/s),
- Lubricant: mineral oil L-AN 46 of kinematic viscosity 46 mm²/s at 40°C,
- Lubricant supply temperature: 22°C.

Tests at selected speeds and loads were carried out until the thermal stabilization was reached. The bearing eccentricity was measured using inductive sensors. Two sensors were located horizontally and two were situated vertically. As a zero position, the contact between shaft and bearing were assumed. After the speed and thermal

stabilization was reached, a new position of the bearing was noticed. The x and y coordinates were calculated and then the eccentricity. The oil temperature was measured in some selected points by the temperature sensors. In **Fig. 2**, a photograph of the smooth journal bearing elements is presented.

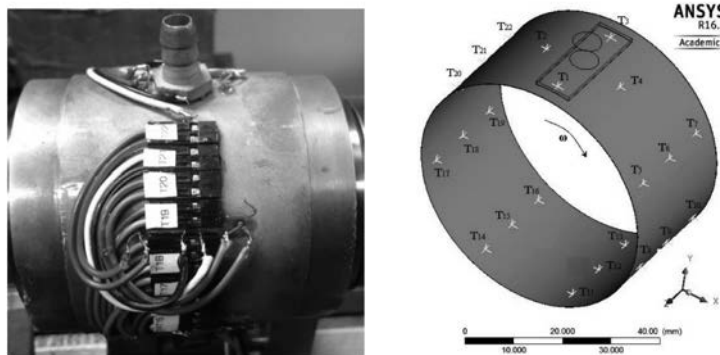


Fig. 2. Photograph of the bearing with temperature probes (a) and scheme of bearing clearance with points of oil temperature measurements (b)

Rys. 2. Zdjęcie panewki z czujnikami temperatury (a) i schemat szczeliny smarowej z punktami, w których mierzono temperaturę oleju (b)

RESULTS AND DISCUSSION

The model of the bearing clearance was verified with the special stand application. Validations of the model applied in the simulation were conducted for two parameters: the load carrying capacity and the oil temperature. In **Fig. 3**, the graph with temperature values measured at selected points is presented, and the load capacity values obtained in modelling and in experiments are shown in **Fig. 4**.

The difference in the temperature values were up to 8 K, which is less than 3%, but the load carrying capacity

obtained in the experiment was up to 12% greater than that in simulations. The simulated load carrying capacity of the optimum grooved series was lower than that of smooth journal bearing by about 18% [L. 14].

After successful model validation, the simulations of the smooth and grooved journal bearings were extended to find the static characteristics at different operating conditions and bearing geometry. Due to the groove presence, the decrease in oil temperature was expected, and, with a smaller bearing clearance, the higher temperature values were obtained. Maximum temperature values in oil film are presented in **Fig. 5**.

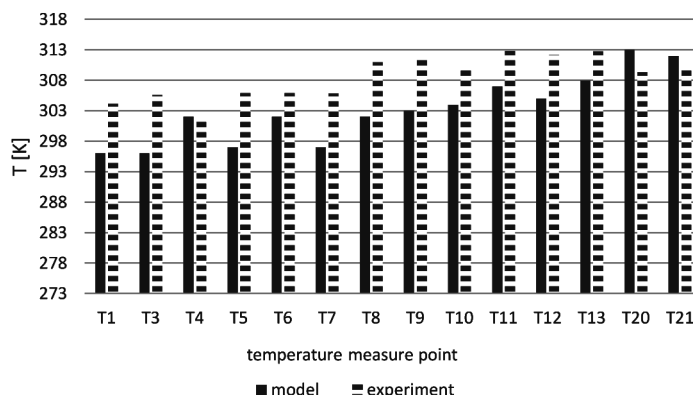


Fig. 3. Temperature values in selected points measured at sliding speed $V = 1.65$ m/s, relative eccentricity $\varepsilon = 0.76$ and relative clearance $\psi = 0.002$ (smooth journal bearing)

Rys. 3. Wartości temperatur w wybranych punktach łożyska mierzone przy prędkości poślizgu $V = 1,65$ m/s, mimośrodowości względnej $\varepsilon = 0,76$ i względnym luzie $\psi = 0,002$ (łożysko gładkie)

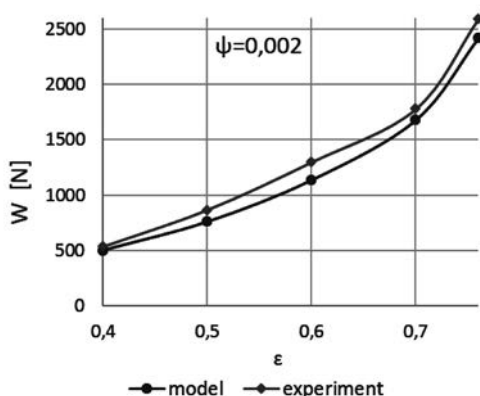


Fig. 4. Load carrying capacity obtained in model and experimental investigation for smooth journal bearing at different relative eccentricities

Rys. 4. Nośność łożyska gładkiego obliczona z modelu i uzyskana w badaniach eksperymentalnych przy różnych mianośrodowościach względnych

At the small eccentricity, the high oil temperature values correspond to greater shear stresses; however, at the high eccentricity, the temperature increase is due to local thinning of the oil film. When analysing the temperature graphs, an interesting fact was found concerning the range of lower temperatures. The range of lower operating temperatures is broader for grooved journals compared to conventional journals. In most cases, the groove on the journal surfaces leads to a maximum temperature decrease. The maximum temperature reduction may be explained by the cooling ability of the oil that is transported in grooves. This hypothesis seems to be confirmed by the increased flow rate in grooved journal bearings in comparison to the flow rate in smooth ones (Fig. 6).

With the increase of relative eccentricity ϵ from 0.1 to 0.8, the flow rate increased in all examined series, and the flow rate was greater when the grooves were present on the journal. The greatest value of oil flow rate was observed for the biggest relative clearance $\psi = 0.003$,

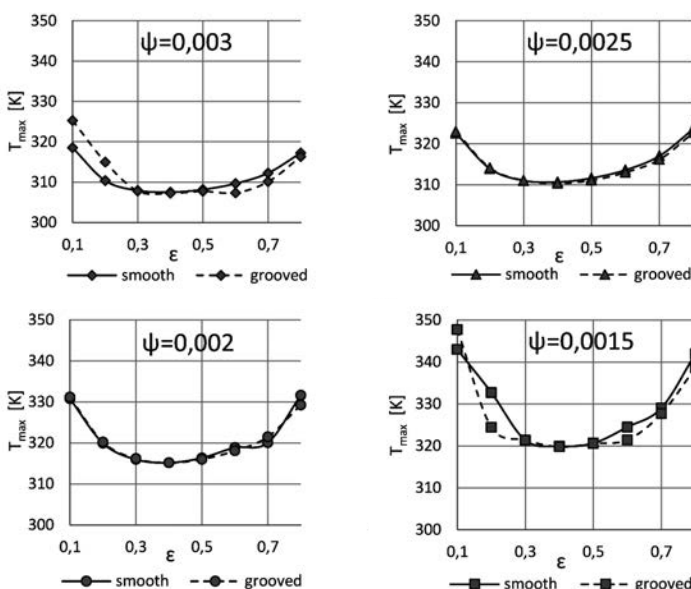


Fig. 5. The influence of relative eccentricity ϵ on the maximum oil temperature T_{max} [K] at different relative bearing clearance for smooth and grooved journals (results from simulation)

Rys. 5. Wpływ mianośrodowości względnej ϵ na maksymalną wartość temperatury oleju T_{max} [K] przy zróżnicowanym względnym luzie łożyskowym dla łożysk gładkich i z rowkiem (badania teoretyczne)

and there the largest difference between grooved and smooth series, especially at ϵ equal to 0.7 and 0.8, was also found. The increase in oil flow rate in the case of the groove may be explained by the creation the paths for the oil movements. When relative clearance was equal to 0.0015, the rate flow was the smallest compared to other series, and the grooved journal bearing had a greater q_0

than the smooth one by up to 13%, while at $\psi = 0.003$, the difference amounted to 19%. Texture creations like dimples or grooves may influence the load carrying capacity in a negative or positive way. The load carrying capacity was defined as an integral of film pressure at a given eccentricity. The results of load capacity for smooth and grooved journals are presented in Fig. 7.

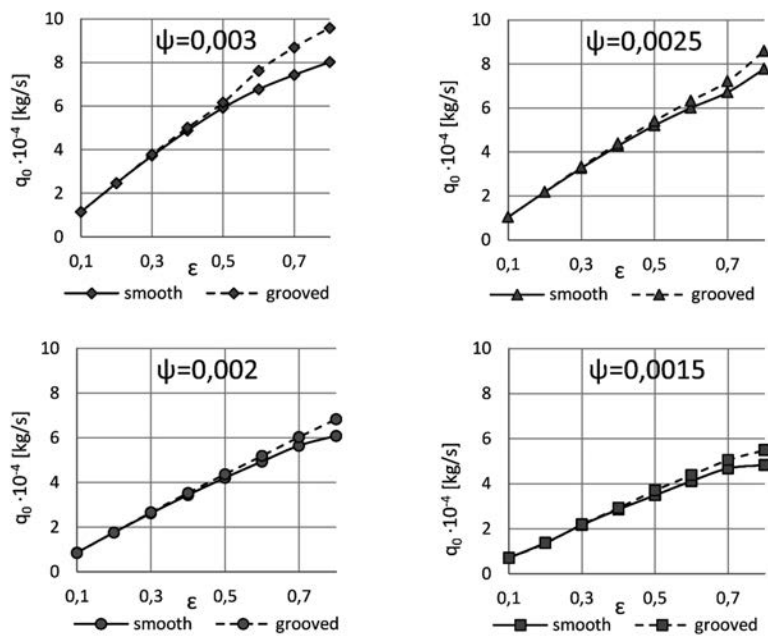


Fig. 6. The influence of relative eccentricity ε on oil flow rate q_0 [kg/s] at different relative bearing clearance for smooth and grooved journals (results from simulation)

Rys. 6. Wpływ mimośrodkowości względnej ε na wydatek oleju q_0 [kg/s] przy zróżnicowanym względnym luzie łożyskowym dla łożysk gładkich i z rowkiem (badania teoretyczne)

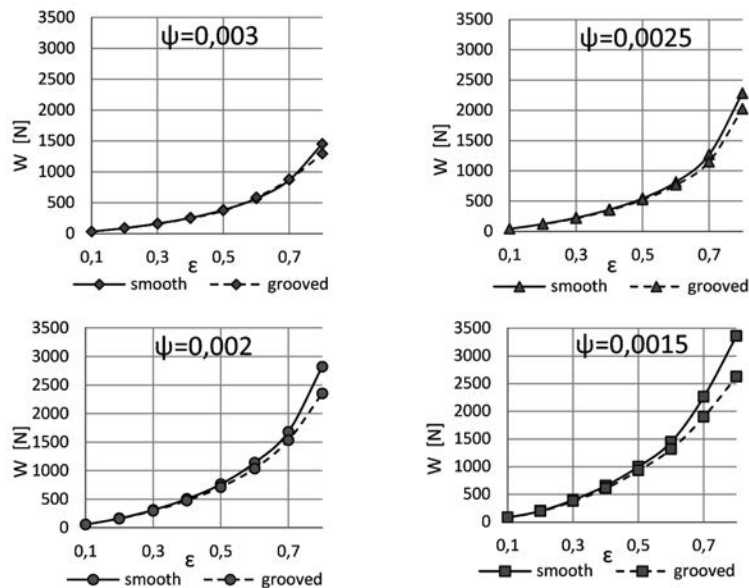


Fig. 7. The influence of relative eccentricity ε on load carrying capacity W [N] at different relative bearing clearance for smooth and grooved journals (results from simulation)

Rys. 7. Wpływ mimośrodkowości względnej ε na nośność łożyska W [N] przy zróżnicowanym względnym luzie łożyskowym dla łożysk gładkich i z rowkiem (badania teoretyczne)

The load carrying capacities of conventional journal bearings in comparison to grooved ones were greater in all examined cases. The differences in bearing capacity values became higher with the increase in eccentricity. Due to the decrease of load carrying surface that was

reduced by the grooves and also because the oil had a specific corridor to flow in, the load carrying capacity of grooved journal bearing was smaller. On the other hand, the oil temperature was mainly lower than that of smooth bearings, which influenced the oil viscosity

but did not compensate for the negative effect of the grooves on the load carrying capacity of clean oil. The greatest decrease in the load bearing capacity of the oil because of groove presence on journal surface was 22% compared to conventional series. Taking into account that this grooved series had over 2-times greater abrasive

wear resistance in contaminated oil, the decrease in the load carrying capacity might not be the only decisive criterion on the application or on the limitation.

Figure 8 presents the pressure curves at different relative eccentricity ϵ starting from 0.1 to 0.8.

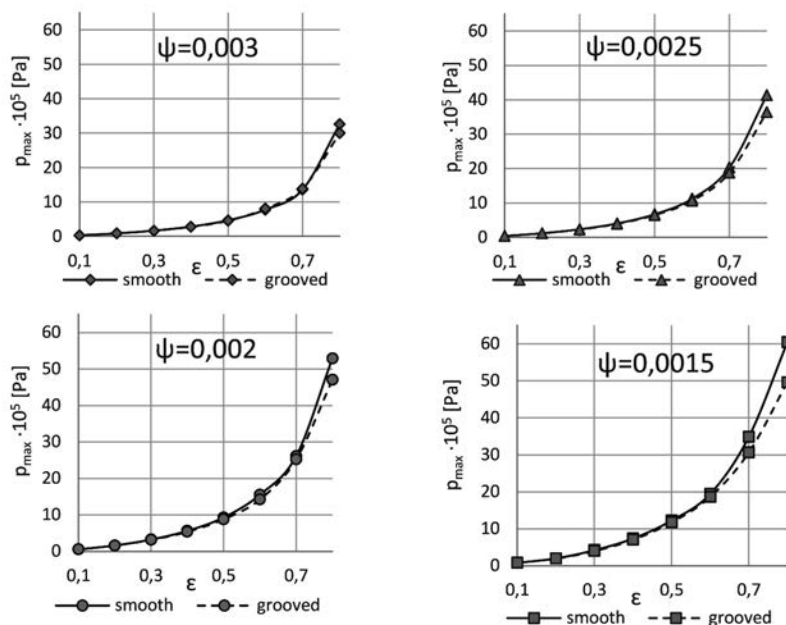


Fig. 8. The influence of relative eccentricity ϵ on max oil pressure p_{max} [Pa] at different relative bearing clearance for smooth and grooved journals (results from simulation)

Rys. 8. Wpływ mimośrodowości względnej ϵ na maksymalną wartość ciśnienia p_{max} [Pa] przy zróżnicowanym względnym luzie łożyskowym dla łożysk gładkich i z rowkiem (badania teoretyczne)

Graphs show maximum pressure values for four series of relative clearance ψ in the range of 0.0015 – 0.003 and for conventional and grooved journal bearings. When the eccentricity was small (lower than 0.5), the values of max oil pressure in the bearing clearance were similar for the smooth and grooved journals. When increasing the relative eccentricity, the gap between maximum pressure values of smooth and grooved journals also increased, and the highest difference of about 1 MPa was obtained at $\epsilon = 0.8$ and $\psi = 0.0015$. Generally, grooves on the journal surface caused a decrease in maximum pressure values compared to p_{max} in the oil clearance of conventional journal bearings. With the decrease in the bearing clearance, the oil pressure significantly increased for smooth and grooved journal cases. The growth in max oil pressure was almost double, comparing p_{max} values when $\psi = 0.0015$ and $\psi = 0.003$.

CONCLUSIONS

The creation of grooves in a journal caused the increase in the oil flow rate, and the increase in eccentricity also increased the flow rate, while the load capacity was lower compared to that of conventional journal bearings. The greatest decrease in load capacity was achieved at the highest eccentricity ratio $\epsilon = 0.8$ and the smallest relative clearance $\psi = 0.0015$. The maximum temperature of oil in the bearing clearance with the grooved journal was usually smaller than that of the smooth journal. The range of lower operating temperatures was broadened due to the presence of the groove when the relative clearance was the smallest ($\psi = 0.0015$). But in this case and at the highest relative eccentricity ($\epsilon = 0.8$), the greatest decrease in maximum oil pressure of 1 MPa was also obtained.

REFERENCES

1. Hirayama T., Sakurai T., Yabe H.: A theoretical analysis considering cavitation occurrence in oil-lubricated spiral-grooved journal bearings with experimental verification, *Transactions of the ASME, Journal of Tribology* 126, pp. 490–498 (2004).
2. Rao T.V.L.N., Sawicki J.T.: Stability characteristics of herringbone grooved journal bearings incorporating cavitation effects, *Transactions of the ASME, Journal of Tribology* 126, pp. 281–287, (2004).
3. Jang G.H., Chang D.I.: Analysis of a hydrodynamic herringbone grooved journal bearing considering cavitation, *Transactions of the ASME, Journal of Tribology* 122, pp. 103–109, (2000).
4. Bootsma J.: The gas liquid interface and the load capacity of helical grooved journal bearings, *Transactions of the ASME, Journal of Lubrication Technology* 95, pp. 94–100, (1973).
5. Bootsma J., Tieleman L.P.M.: Conditions of leakage-free operation of herringbone grooved journal bearings, *Transactions of the ASME, Journal of Lubrication Technology* 99, pp. 215–223, (1977).
6. Sep J., Pawlus P., Gałda L.: The effect of helical groove geometry on journal abrasive wear. *Archives of Civil and Mechanical Engineering* 13, pp. 150–157 (2013).
7. Sep J., Pawlus P., Dzierwa A.: The analysis of abrasive wear of the helical grooved journal bearing. *Key Engineering Materials* 527, pp. 173–178, (2013).
8. Tala-Ighil N., Fillon M.: A numerical investigation of both thermal and texturing surface effects on the journal bearings static characteristics. *Tribology International* 90, pp. 228–239 (2015).
9. Brizmer V., Kligerman Y.: A laser surface textured journal bearing. *Transactions of the ASME, Journal of Tribology* 134, 031702-1-031702-9 (2012).
10. Tonder K.: Inlet roughness tribodevices: dynamic coefficients and leakage. *Tribology International* 34, pp. 847–852 (2001).
11. Ryk G., Etsion I.: Testing piston rings with partial laser surface texturing for friction reduction. *Tribology Transaction* 48 (4), pp. 583–588 (2005).
12. Etsion I.: Modeling of surface texturing in hydrodynamic lubrication. *Friction* 1 (3), pp. 195–209 (2013).
13. Etsion I., Halperin G., Brizmer V., Kligerman Y.: Experimental investigation of laser surface textured parallel thrust bearings. *Tribology Letters* 17 (2), pp. 295–300 (2004).
14. Sep J., Tomczewski L., Gałda L., Dzierwa A.: The study on abrasive wear of grooved journal bearings. *Wear* 376–377, pp. 54–62 (2017).
15. Sep J.: The oil film properties in journal bearings with non-typical geometry, Rzeszow University of Technology, Rzeszow (2006) (in Polish)
16. Sep J.: Journal bearing with an intensive axial oil flow – experimental investigation. *Scientific Problems of Machines Operation and Maintenance* 2 (154), pp. 21–31 (2008).
17. ANSYS FLUENT “Theory Guide”.